

Stator Fault Detection and Faulty Phase Identification in Network/Inverter-fed Induction Machines using Negative Sequence Current Component

Mohammad Hossein Nazemi¹, Farhad Haghjoo^{1,*}, Sérgio Cruz², Monia Bouzid³

¹ Faculty of Electrical Engineering, Shahid Abbaspour School of Engineering, Shahid Beheshti University, Tehran, Iran

² Department of Electrical and Computer Eng., University of Coimbra, 3030-290 Coimbra, Portugal, and Instituto de Telecomunicações, 3030-290 Coimbra, Portugal

³ Laboratory of Electrical Systems, National School of Engineers of Tunis, University of Tunis EL Manar, and the National School of Engineers of Carthage, University of Carthage, Tunis, Tunisia

ARTICLE INFO

Article history:

Received 18 June 2023

Received in revised form 16 August 2023

Accepted 23 August 2023

Keywords:

Induction motors

Stator turn-to-turn faults

Fault detection

Faulty phase identification,

Negative sequence current component



Copyright: © 2023 by the authors. Submitted for possible open access publication under the terms and conditions of the Creative Commons Attribution (CC BY) license (<https://creativecommons.org/licenses/by/4.0/>)

ABSTRACT

This paper proposes a non-invasive negative sequence impedance-based technique to detect stator turn-to-turn faults (STTFs) and identify the related faulty phase at early stages based on the tracking the magnitude and angle variations of the negative sequence current component generated due to STTFs. To extract these indicators, a simplified steady-state negative sequence equivalent circuit of the induction motor is used. To neutralize the effect of various produced disturbances by the inherent non-ideal construction of the machine and also unbalanced feed voltage to the STTF diagnosis, they will be estimated and removed from the main obtained component. It is shown experimentally that the introduced technique is independent of mechanical loading level (load variations) and is applicable for network or inverter-fed motors as well. Online fault detection and faulty phase identification, as the most important goals of the protection plan, are accessible by defining an appropriate threshold for the magnitude and allowable range of angle variation of the introduced criterion, respectively.

The performance of the method is evaluated by simulation as well as multiple experimental tests. The experimental results have shown that from the sensitivity point of view, even weak faults are detectable by such a technique. Also, the obtained tests showed that such technique is robust, reliable and secure in the face of unbalanced voltage sources and load level variations. In addition, the performance of this method for the inverter-fed mode showed that the related sensitivity will be increased in such a condition.


1. Introduction

More than 70% of the electricity required by industry is used to operate electric drives. Among them, around 67% are based on induction machines (IM) [1, 2]. IMs are exposed to several thermal, electrical, ambient, and mechanical (TEAM) stresses, depending on the

industry's type of operation, driven load, and environment. Statistics have shown that despite their ruggedness and simplicity in construction, the motor annual failure rate is conservatively estimated at 3-5% per year. There are up to 12% in extreme cases, as in cement, mining, pulp, and paper industries [3]. Motor

* Corresponding author

E-mail address: f_haghjoo@sbu.ac.ir

 <https://www.orcid.org/0000-0001-5442-4878>

<http://dx.doi.org/10.52547/ijrtei.1.1.105>

failures cause unexpected outages and possibly disrupt production and impose unforeseen costs such as repairs, replacements, and installation on the plant. Thus, proper protection is required to minimize the motor failure rate, prevent further damage to the equipment and ensure minimum outage time and productivity targets [4, 5].

Based on the results of IEEE and EPRI surveys on motor reliability and significant causes of motor failures, on average, about 33% of faults are related to the stator and rotor windings [6]. In the case of STTFs, the induced voltage in the shorted turns may lead to a circulating current up to twice the locked-rotor current [7]. If the protection system does not clear the fault, it can propagate and lead to more severe faults, such as phase to ground or phase-to-phase faults. In medium voltage motors, due to the high short-circuit power of the network, an uncleared earth fault can cause irreparable damage to the machine stator core [8].

The existing methods to detect STTFs can be classified into two main categories: invasive and non-invasive. Invasive techniques mainly use pre-fabricated sensors to monitor variations in the magnetic flux density, stray flux, temperature, and frame vibrations [9, 10]. Non-invasive or sensorless fault detection methods, which monitor the motor condition using only the terminal current and voltage signals, are preferred due to their reasonable cost and independence from the use of special sensors that may be difficult to fit into the motor. Although the invasive techniques have some advantages from the security, sensitivity, and reliability viewpoints, they generally require changes to the machine's construction, which sometimes has its own complexities in the field.

Some of the most common non-invasive techniques are:

- the motor current signature analysis (MCSA), based on the spectrum analysis of the motor supply current [11-13];
- the Park's vector approach [14, 15];
- the instantaneous active and reactive power analysis [16, 17];
- artificial intelligence-based (AI) techniques [18, 19], using raw data obtained from the speed, torque or negative sequence current signals;
- other techniques that use more sophisticated current signal processing techniques, such as the Discrete Wavelet Transform or the Hilbert Transform [20-22].

However, since this work proposes a model-based approach using the IM negative sequence equivalent circuit and the related current components to detect STTFs, previous methods closely associated with the proposed one are analyzed in more detail.

As stated in several papers, some of the primary causes of the negative sequence current component (\bar{I}_2) flowing in the stator windings of the IM are the imbalance of the supply voltages and the machine's inherent asymmetries caused by its non-ideal construction. The degree of imbalance of the supply voltages, measured as a percentage by the unbalance voltage factor $UVF = (V_2/V_1) \times 100\%$ has a significant impact on the motor performance, and even if relatively low, it can impose a lot of thermal stresses on the machine [23-25]. On the other hand, one of the primary effects of an STTF is the disruption of the symmetry of the stator currents by

introducing an additional negative sequence current component. The separation of the effects of an STTF of the impact of unbalanced supply voltages and inherent motor asymmetries in the negative sequence current component is thus a major challenge for a correct decision in the fault detection process.

It was shown in [26] that as the negative sequence current (I_2) is not significantly affected by load level variations, it can be used as a more accurate and reliable indicator of STTFs. In [27], by using a reduced negative sequence model of the IM, the effective negative sequence impedance is assumed unaffected by the load level for a small number of shorted turns. Accordingly, the residual negative sequence current was used to introduce a fault criterion. Also, a self-tuning technique measured the intrinsic motor asymmetries to obtain a lookup table (as a function of I_1 and V_1) due to their sensitivity against voltage and slip variations in the mentioned paper. Although this method exhibits a high accuracy in detecting STTFs, the effect of the unbalanced voltage source (UVS) has not been investigated on the related performance. In addition, an acceptable protection threshold which is covering all non-ideal conditions was not provided. Another drawback is the technique for compensating the intrinsic IM asymmetries, which requires the inspection of each IM individually and using a learning stage to create a lookup table.

In [7], modified steady-state equivalent circuits were proposed for the negative sequence current component and short-circuit current when an IM has an STTF with a fault severity factor μ (defined as the ratio between the number of shorted turns and the number of turns per phase), as shown in Fig. 1.

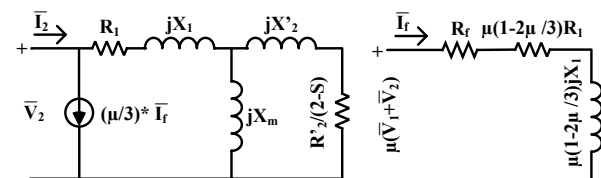


Fig. 1. Steady-state equivalent circuits in [7] for an IM with STTFs: the negative sequence equivalent circuit (left) and the fault current (right).

Since \bar{I}_2 depends on the fault current (\bar{I}_f) as well as the negative sequence voltage (\bar{V}_2), it is given by:

$$\bar{I}_2 = \frac{1}{3} \mu \bar{I}_f + \bar{Y}_2 \bar{V}_2 \quad (1)$$

where \bar{Y}_2 is the negative-sequence admittance of an ideal symmetrical IM. According to those equivalent circuits, the fault current \bar{I}_f is given by:

$$\bar{I}_f = \frac{\mu(\bar{V}_1 + \bar{V}_2)}{\mu \left(1 - \frac{2\mu}{3}\right) [R_1 + jX_1] + R_f} \quad (2)$$

where R_1 , X_1 , and R_f are respectively the stator winding resistance, leakage reactance, and STTF contact resistance. By applying some minor simplifications due to the negligible value of μ and V_2 in comparison with V_1 (maximum 1.5% according to the grid codes of some

countries [28]), it can be concluded that the fault current depends approximately on the positive sequence voltage and stator winding impedance. Moreover, the fault current should always lag the reference voltage by an angle equal to the stator impedance angle (for a dead short-circuit). Although this relation provides a sense of perspective about the magnitude of the fault current, a detailed analysis of machine behavior in the nonlinear zone is very complicated due to the saturation of the stator core during the fault, which will definitely have a direct impact on the fault current angle or direction [29]. Moreover, the leakage reactance depends on the physical location of the faulted turns along the stator winding. In [7], and according to (1) and (2), \bar{I}_2 is a function of \bar{V}_1 and \bar{V}_2 and load-dependent coefficients \bar{K}_1 and \bar{K}_2 as $\bar{I}_2 = \bar{K}_1 \bar{V}_1 + \bar{K}_2 \bar{V}_2$. Using some datasets obtained at different loads, these coefficients can be estimated and a lookup table built in order to neutralize the effects of the inherent motor asymmetries and UVS, while such lookup table cannot be generalized to other IMs. In addition, the evaluation was done in perfectly linear conditions and only considering one value of the UVF. Lastly, a reliable method to determine the faulty phase was not provided. Following a slightly different approach, in [30, 31], the variations of the off-diagonal elements of the admittance matrix for the IM's positive and negative sequence components are used to detect STTFs. This technique was applied to line-fed machines and inverter-fed ones [32-35]. Some of the undeniable advantages of such a diagnostic method are high accuracy, the study of the loading effects, modifying the non-ideal machine construction, and the limited unbalance voltage consideration in estimating the initial conditions. In contrast, complexity, the high computational burden, the need to repeat the learning stage for each particular IM, the lack of providing a reliable threshold value, and the absence of an algorithm to identify the faulty phase are the main drawbacks of this approach.

In [36-38], a semi-empirical formula based on theoretical and experimental data is recommended to compensate the inherent asymmetry of IMs, voltage variations, and other non-ideal dependencies. Despite extensive research and acceptable conclusions to provide a unique threshold to detect STTFs, there is a need for further improvements. In particular, other types of IMs, such as wound-rotor induction machines (WRIMs), have to be considered, and the variation of the effective negative sequence impedance angle due to the contribution of STTF current definitely has a great impact on the security and reliability of the pre-formed database.

In [39-42], the negative sequence current tracking is also used as the STTF detection criterion. In [39], it is theoretically proved that the negative sequence current angle ($\angle \bar{I}_2$) as the result of STTF location is as follows:

$$\angle \bar{I}_2|_{STTF@A} = 0^\circ, \angle \bar{I}_2|_{STTF@B} = 120^\circ, \angle \bar{I}_2|_{STTF@C} = 240^\circ \quad (3)$$

Along with the innovations made and a specific glance at the $\angle \bar{I}_2$ behavior, it is explicitly concluded that $\angle \bar{I}_2$ is ineffective against slip and voltage variations, which is not compatible with simulation and experimental results in the same reference and [42]. This incompatibility stems from inherent asymmetry and the combination of

loading and UVS effects that were not addressed in that paper. However, limited voltage variation in terms of magnitude and angle and non-calibrated measuring sensors effects are studied to some extent. Moreover, in [39, 40], any acceptable and secure threshold for STTF detection was not proposed.

There are other techniques based on neural networks [43-45], zero sequence voltage monitoring [46], and effective negative sequence impedance [47, 48]. A general comparison of all relevant techniques is summarized in Table I.

In this paper, a more comprehensive strategy is proposed to detect the STTFs in IMs based on the relative magnitude and angle of \bar{I}_2 for STTF detection and faulty phase identification in an online condition by the neutralization of the UVS related current component. Indeed, this paper uses a model-based approach to detect and locate STTFs in IMs. The method is based on monitoring the magnitude, and angle of the negative sequence current component caused by the circulation of the short-circuit current in the shorted turns, thus providing a reliable fault signature of STTFs.

The originality of this work can be explained by the following items:

- Extraction of the negative sequence faulty current component caused by the short-circuit current flowing in the branch containing the shorted turns by using the simplified model, which results from a modification introduced in the model (Fig. 2).
- Presentation of an efficient and generalized methodology to set the fault threshold level, leading to accurate STTF detection without false alarms. This threshold setting can be used with all types of IMs and takes into account all non-ideal conditions of the machine to diagnose STTFs with high reliability, accuracy, and sensitivity.
- Identification of the faulty phase by using the angle of the purified negative sequence current, while whole the trigonometric circle is divided to three symmetric regions for three phases to determine the faulty phase, as well.

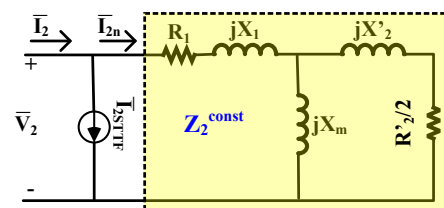


Fig. 2. The proposed simplified negative sequence equivalent circuit of IMs.

In continue, the proposed method is described in the Sec. 2. The simulation and experimental results are presented in Sec. 3 and Sec. 4, respectively, and finally, the paper is concluded in Sec. 5.

2. Proposed method to diagnose STTFs

According to the negative sequence equivalent circuit of Fig. 2, the equivalent rotor resistance referred to the stator side is approximately equal to half the rotor resistance ($R'_2/2$) since the slip “s” is very small ($s \leq 5\%$). Thus, it can be considered that in the proposed

simplified model of the healthy negative sequence impedance is a constant impedance \bar{Z}_2^{const} , insensitive to the motor load conditions. It should be noted that \bar{Z}_2^{const} can be easily calculated from the rated values in the machine nameplate or from the general no-load and lock-rotor tests specified in IEEE Std 112 [49].

2.1. STTF Detection Procedure

As illustrated in Fig. 2, the simplified negative sequence equivalent circuit, supplied by the negative sequence voltage \bar{V}_2 , is composed of two branches in parallel: the negative sequence impedance \bar{Z}_2^{const} branch and the negative sequence faulty current (\bar{I}_{2STTF}) one, which represents the branch containing the effects of the STTF.

Table I. Summary of negative and zero sequence oriented techniques

Reference No.	Fault Index	Fault Type	Inherent Asymmetry Compensation Technique	Considering the Effect of Unbalance Voltage Source	Considering the Loading Level	Threshold	Faulty Phase Identification	Security Investigation Against Rotor Faults
[2]	$ I_2 $	STTF	Complex constant K estimation ($I_2 = K_1V_1 + K_2V_2$) & Look-up table	Complex constant K estimation ($I_2 = K_1V_1 + K_2V_2$) & Look-up table	✓	✗	✗	✗
[27]	$ I_2 $	STTF	Look-up table	✗	✓	✗	✗	✗
[32-35]	Z_{np} (off-diagonal element of admittance matrix)	STTF	Estimation of Z_{np} in two different stages of V_2 & slip	Estimation of Z_{np} in two different stages of V_2 & slip	✓	✗	✗	✗
[36-38]	$ I_2 $	STTF	Z_2 effective & thermal effect minimization ($I_2 = \frac{V_2 \sin \theta_2}{X_{h2}}$)	The semi-empirical quadratic function of healthy reactance (X_{h2}^2)	✓	✓	✗	✗
[39]	$\angle I_2$	STTF	✗	Considering limited test points of injected unbalance voltage	✗	✗	✓	✗
[40]	$ I_f $ & $\angle I_2$	STTF	✗	✗	✗	✗	✓	✗
[41]	$ I_2 $ & $\angle I_2$	STTF	✗	✗	✓	✗	✓	✗
[42]	$ I_2 $	STTF	Look-up table	Look-up table	✗	✗	✗	✗
[43-45]	$ I_2 $	STTF	Neural network	Neural network	✓	✗	✗	✗
[46]	$ V_0 $	STTF	Using summation of the fundamental component of voltages	✗	✗	✗	✗	✗
[47, 48]	Z_2^{eff}	STTF	✗	✗	✗	✗	✗	✗
This Paper	$ I_{2STTF} $ & $\angle I_{2STTF}$	STTF	✓	✓	✓	✓	✓	✓

Hence, the total negative sequence current \bar{I}_2 generated in a faulty motor is the sum of the negative sequence current \bar{I}_{2n} flowing in the negative sequence impedance \bar{Z}_2^{const} (healthy part) and the negative sequence current \bar{I}_{2STTF} flowing in the faulty branch as given by:

$$\bar{I}_2 = \bar{I}_{2STTF} + \bar{I}_{2n} \quad (4)$$

Using the three measured stator currents and voltages of the motor, the total negative sequence current \bar{I}_2 and the negative sequence voltage \bar{V}_2 are calculated at any moment by applying the Fortescue transformation or any other technique [50].

In healthy operating conditions, the current in the constant negative sequence impedance branch \bar{I}_{2n} can be calculated by:

$$\bar{I}_{2n} = \bar{V}_2 / \bar{Z}_2^{const} \quad (5)$$

This current is not expected to be null even when $\bar{V}_2 = 0$ because of the different non-idealities of the machine mentioned in the introduction.

When the machine operates with an STTF, the STTF contribution branch's current \bar{I}_{2STTF} will be assessed simultaneously by subtracting \bar{I}_{2n} from the total negative sequence current \bar{I}_2 circulating in the machine as follows:

$$\bar{I}_{2STTF} = \bar{I}_2 - \bar{I}_{2n} \quad (6)$$

Hence, the variations in the amplitude and angle of \bar{I}_{2STTF} will be considered as the main criteria for STTF detection and faulty phase identification.

On the other hand, it is worth noting that industrial protection relays commonly protect the motor using a fault detection criterion (FDC) based on the ratio between I_{2STTF} of and positive sequence current components magnitude (I_1). By analogy, in this work, the FDC used is defined as:

$$FDC = (I_{2STTF} / I_1) \times 100\% \quad (7)$$

It should be noted that due to the maximum permissible UVF of the grid (which can reach 1.5% in some countries [28]), due to the inherent machine asymmetries and even the minor effects of the load level variation on the actual value of the negative sequence impedance of the machine, in practical conditions \bar{I}_{2STTF} will never be zero. As such, it is mandatory to choose an adequate and secure threshold (Th_{STTF}) to ensure accurate fault detection. The proposed threshold is defined based on several tests performed under different load conditions and for different negative sequence voltage component levels. The choice of the threshold value is addressed in the simulation and experimental sections.

Evaluating these experimental test results for adjusting the threshold value has the advantages of (i) practically eliminating any training process algorithm, (ii) the need to build a look-up table to compensate for non-idealities, (iii) the effects of unbalanced voltage sources, and (iv) the minimization of thermal effect aspects that were used and discussed in detail in previous references [36-38]. With the selected fault threshold value (Th_{STTF}), the STTF detection procedure is based on the monitoring and

comparison of the FDC with Th_{STTF} . If the FDC is smaller than Th_{STTF} , the machine is considered in healthy condition. Otherwise, an STTF has occurred and the fault location must be traced for the second step of the diagnosis process.

2.2. Faulty Phase Identification

Once an STTF is detected, the identification of the faulty phase will be based on the monitoring of the angle $\angle \bar{I}_{2STTF}$ of the negative sequence faulty current.

In the case of an STTF, a major portion of \bar{I}_2 flows in the parallel STTF branch of the proposed simplified equivalent circuit of Fig. 2. Thus, $\angle \bar{I}_{2STTF}$ is close to $\angle \bar{I}_2$ As mentioned in [41], for an STTF occurring in phases A, B or C, $\angle \bar{I}_2$ is predicted to be 0° , 120° , and -120° , respectively, and an identical behavior could be anticipated for $\angle \bar{I}_{2STTF}$. However, in real conditions, $\angle \bar{I}_{2STTF}$ is located around (not exactly on) the corresponding phase axes (0° , 120° , and -120°). This happens because the assumptions based on which the results in [41] were obtained are only an approximation of reality and do not reflect the exact electromagnetic behavior of the machine under the presence of an STTF. The neutral point of the stator windings, in a star-connected machine, will be shifted from its normal position when an STTF appears, and the magnetic axis of the shorted turns also does not coincide in many cases with the magnetic axis of the healthy phase windings. In addition, there is a reduction in the phase voltage of the winding affected by the fault as a consequence of the decrease in the effective number of turns of that winding. The circulation of a reverse current in the shorted turns reduces the linkage flux in a wide portion of the faulty winding, thus moving the operating point downwards in the B-H curve. Such variations in this region will also change the operating points of the other phase windings (healthy ones) in the common coil areas, as the coils of different phases overlap partially and share some core sections.

Accordingly, the negative sequence equivalent circuit can only be considered approximately under the presence of STTFs. It has an acceptable accuracy when the machine is in healthy conditions, i.e., when $\bar{I}_{2STTF} = 0$. In this work, this circuit is used only to calculate \bar{I}_{2n} and obtain $\bar{I}_{2STTF} = \bar{I}_2 - \bar{I}_{2n}$. If \bar{I}_{2STTF} is higher than the threshold value, an STTF has been confirmed. Afterward, when an STTF is detected, the faulty phase can be identified according to the sector in which $\angle \bar{I}_{2STTF}$ is located:

$$\begin{aligned} -60^\circ < \angle \bar{I}_{2STTF} < 60^\circ &\rightarrow \text{STTF is in phase A} \\ 60^\circ < \angle \bar{I}_{2STTF} < 180^\circ &\rightarrow \text{STTF is in phase B} \\ 180^\circ < \angle \bar{I}_{2STTF} < 300^\circ &\rightarrow \text{STTF is in phase C} \end{aligned}$$

2.3. Flowchart of the Proposed Method

According to the descriptions mentioned above, the entire procedure for the diagnosis of STTF can be illustrated with the aid of a logical flowchart depicted in Fig. 3. Based on this flowchart, using an appropriate threshold (Th_{STTF}) and an empirical range of angular changes around the central axis of each phase (0° , 120° , and -120°), an effective STTF detection is guaranteed, and the faulty phase can be identified without any overlap.

The fault detection process and faulty phase identification are summarized in the following steps:

- Data acquisition and calculation of \bar{I}_2 and \bar{I}_{2n} ;
- Extraction of \bar{I}_{2STTF} by using (6);
- Calculation of FDC and comparing it with Th_{STTF} ;
- If FDC exceeds Th_{STTF} , an STTF is confirmed;
- In a faulty case, the identification of the defective phase depends on the value of $\angle \bar{I}_{2STTF}$ as mentioned in the previous subsection.

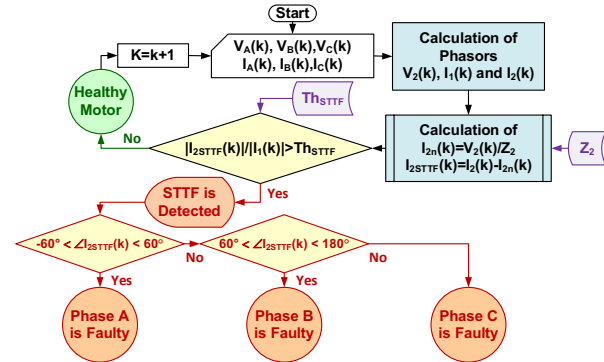


Fig. 3. Flowchart of the proposed diagnostic method.

3. Simulation results

To validate the proposed diagnostic method, a WRIM was simulated in a finite element software package (Ansys Maxwell ver.16). The simulated WRIM is similar, although not precisely equal at the fundamental frequency of 50 Hz.

The negative sequence impedance of the simulated WRIM is $\bar{Z}_{2,no-load}^{const} = 9.705 \angle 82.30^\circ \Omega$ and $\bar{Z}_{2,full-load}^{const} = 8.534 \angle 81.10^\circ \Omega$ and for no-load and full-load conditions, respectively.

To evaluate the weak points of previous studies and also highlight the advantages of the proposed diagnostic approach, the fault indices are studied with the machine under STTFs in each phase separately (STTF_{5A}, STTF_{5B}, and STTF_{5C}), both in balanced and unbalanced voltage supply conditions (with a permissible UVF=1%). The FDC is calculated considering a constant value for $\bar{Z}_2^{const} = \bar{Z}_{2,full-load}^{const}$.

In Fig. 4, the FDC calculated by (7) (which represents the modulus) and the angle $\angle \bar{I}_{2STTF}$ are plotted in polar coordinates for three different faulty cases (encompassing faults in the three stator phases), for a balanced (blue crosses) and an unbalanced (red circles) voltage supply system, when the machine runs at no-load (left) and full-load (right). The results show that the FDC values are higher for the no-load condition in comparison with the full-load case, which is easily justifiable by the higher positive sequence current component for higher motor load levels, while \bar{I}_{2STTF} is barely independent of the motor load condition. It is also visible the dispersion of the obtained points around the three colored areas being this dispersion more when there is an unbalanced supply voltage in addition to the STTF. In addition, it can be concluded by looking at Fig. 4 that FDCs for all cases is greater than 3.7%, while such a value can be chosen as an appropriate threshold (Th_{STTF}). Moreover, as can be seen, the related fault index angles ($\angle \bar{I}_{2STTF}$) in both conditions are fully compatible with the recommended faulty phase

detection algorithm in the flowchart and go through all non-ideal conditions. Although the results for the full load are focused on the specific regions on the angles zero, 120° and -120° for STTF occurrence on phases A, B, and C respectively (Fig. 4, right), such results for the no-load condition are more distributed due to the lower I_1 in comparison to the I_{2STTF} in the FDC relation. However, the expected geometric location of these points for each specific STTF did not interfere with the adjacent areas for the healthy phases. Also, it can result that faulty phase identification may be made with more reliability in the full load than in the no-load conditions.

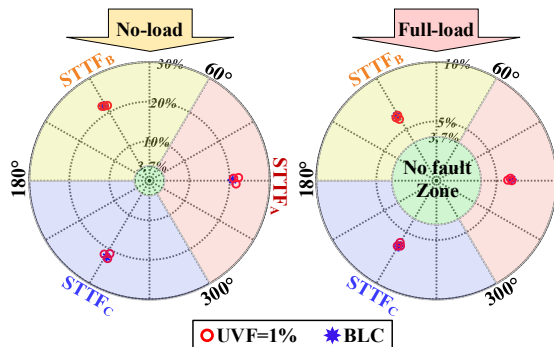


Fig. 4. FDC and $\angle \bar{I}_{2STTF}$ in the face of balanced and unbalanced (with UVF=1%) voltage sources in no-load (left) and full-load conditions for three faulty cases in the three phases (STTF_{5A}, STTF_{5B}, and STTF_{5C}).

4. Experimental results

4.1. Experimental Setup

In the experimental validation of the proposed diagnostic methodology, a three-phase WRIM with the specifications in Table II is used. For higher flexibility, three single-phase variacs (autotransformers) were used in order to control the degree and type of the unbalanced supply voltages applied to the machine in some experiments. The applied voltages and machine supply currents are sensed with three current transformers and three potential transformers and measured using synchronized analog to digital converters with a sampling frequency of 5 kHz. A low voltage synchronous generator that supplies a three-phase resistor bank is coupled to the WRIM shaft in order to control its mechanical load by adjusting its field current. Several taps are connected to different points along the three stator windings of the WRIM to allow the introduction of STTFs in an online condition. A schematic diagram and a picture of the experimental setup are shown in Fig. 5.

Table II. WRIM characteristics

Par.	Value	Par.	Value	Rat.	Value	Rat.	Value
R_1	2.606 Ω	X'_2	2.833 Ω	P_r	2.2 kW	Poles	4
R'_2	4.098 Ω	X_m	40.889 Ω	V_r	380 V (L-L)	n_r	1360 rpm
X_1	2.833 Ω	Z_2^{osnt}	7.15 $\angle 51.21^\circ \Omega$	P.F.	0.75	Turns	216

4.2. Unbalanced Voltage Source in a Healthy Machine

First, the effects of UVS applied to a healthy machine are evaluated, namely the variations of $\angle \bar{I}_2$ w.r.t the

imbalance voltage deviation direction, as shown in Fig. 6 using polar coordinates. The voltage imbalance was created by decreasing the voltage amplitude in each phase separately. For an imbalance in phase A, $\angle \bar{I}_2$ varies somewhere along the axis of 180°. Similarly, if the voltage asymmetry is created in phases B and C, $\angle \bar{I}_2$ will be located near or along the axes of -60° and 60°, respectively. These central axes values are opposite (phase-shifted by 180°) to the axes associated with the faults in the corresponding phases, as shown before in Fig. 4. In fact, the axes of each UVS coincide with the phase of the voltage vector of the negative sequence component of the motor supply voltages.

To cover all non-ideal situations and inevitably inaccuracies of the model used for STTF detection, the healthy operation of the machine is characterized by a negative sequence current vector. This vector lies in regions symmetrically built around each of the previously mentioned axes, with an opening of 120° so that they do not overlap, as highlighted by the three colored areas in Fig. 6.

The motor's unbalanced supply voltage is arbitrary in actual operating conditions. In these circumstances, the healthy motor operation can be characterized by a negative sequence current vector that lies in an area of 120° built around the axis defined by the negative sequence component of the supply voltages.

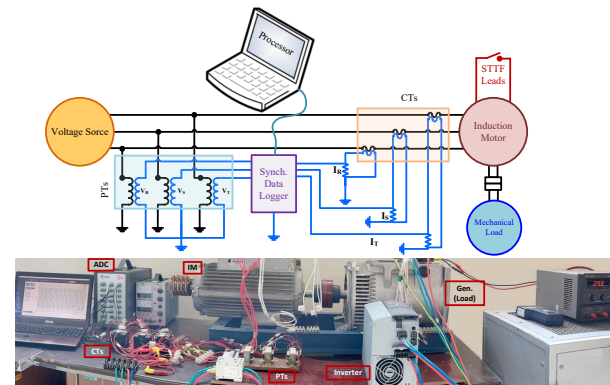


Fig. 5. Schematic diagram and picture of the experimental setup.

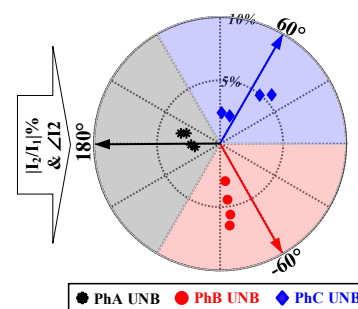


Fig. 6. The variation of $\angle \bar{I}_2$ respect to the imbalance voltage deviation direction (UVF variations are in the range of 0.5~1.7%).

4.3. Negative Sequence Current Components for STTFs

The impact of different STTFs (different numbers of shorted turns) in the negative sequence current components I_2 and I_{2STTF} for two values of the UVF are illustrated in Fig. 7 for different time windows of 100 ms.

All current components were normalized w.r.t I_1 and expressed as a percentage.

As shown, the percent values of I_2 depend on the STTF severity and the degree of imbalance of the supply voltages. However, the calculated I_{2STTF} depends only on the STTF severity, and a linear relationship can approximate such dependency. As seen, by removing the unbalanced voltage source effect on the I_{2STTF} , an approximately linear relationship will be appeared between the FDC value and the fault severity.

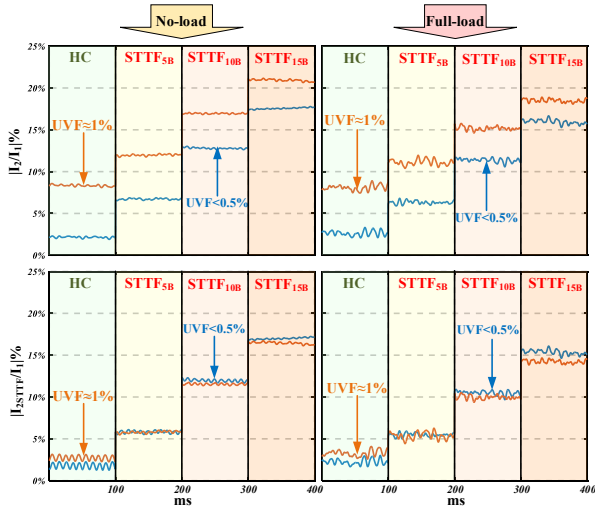


Fig. 7. The percentage of I_2 (top) and I_{2STTF} (down) respect to I_1 at no-load (left) and full-load (right) conditions for different categories of HC and STTFs in almost balanced ($UVF < 0.5\%$, blue) and unbalanced voltage sources (UVF about 1% , red).

4.4. Fault Threshold Level Definition

Similar to other current-based diagnostic techniques, there is the need to define a reliable and secure threshold level to distinguish faulty cases from healthy ones. To determine such threshold level for STTF detection (Th_{STTF}), the motor FDC was evaluated for different voltage unbalances, ranging from the most severe cases ($UVF > 1\%$, up to 1.7%) to the lower ones ($UVF < 0.5\%$), with the motor in healthy conditions. In these tests, the inherent motor constructional asymmetries are taken into consideration. Fig. 8 shows that for the tested motor, both at no-load and full-load conditions, the FDC slightly exceeds 3% for a $UVF \cong 1.7\%$. Accordingly, in order to provide a secure and reliable level for STTF detection, Th_{STTF} is selected 20% more than the maximum value in the healthy condition and is set as 3.7% . Choosing a lower Th_{STTF} ($3.2 \sim 3.7\%$) would increase the sensitivity, decrease security, and vice-versa.

4.5. Detection and Location of STTFs in Real Conditions

To evaluate the performance of the introduced method, three faulty conditions, including $STTF_{5B}$, $STTF_{10B}$, and $STTF_{15B}$ have been applied to the machine running at no-load and rated load conditions. An UVF is also considered and applied as weak ($UVF < 0.5\%$), medium ($0.5\% < UVF < 1.1\%$), and severe ($UVF > 1.1 \sim 1.7\%$). In practice, it is illogical to investigate the effects of unbalanced voltage sources with a $UVF > 1.7\%$. In such cases, the motor

protection would be the responsibility of adequate relays defined by the ANSI standard device numbers [51], namely the 47 (phase balance voltage relay) and 27/59 (under and over-voltage relay). Fig. 9 shows the experimental test results for such conditions. As can be seen, the FDC values for $STTF_{5B}$ are slightly higher than 5% , and the related $\angle \bar{I}_{2STTF}$ are located between 120° and 180° . FDCs for $STTF_{10B}$ is around 10% , and the related $\angle \bar{I}_{2STTF}$ are located in the vicinity of the 120° axis. For $STTF_{15B}$, FDCs are about 15% and the related $\angle \bar{I}_{2STTF}$ is in the range $110 \sim 120^\circ$. Thus, all test points are concentrated in the predicted areas. Moreover, it can be concluded that the FDC values for the faulty cases depend on the STTF severity factor (μ).

To evaluate the methodology's performance for identifying the faulty phase, $STTF_{10A}$ was also applied to the machine, and the results are shown in the 4th column of Fig. 9. As can be seen, similar to the $STTF_{10B}$ case, the obtained FDCs for all test cases are around 10% , and the angle $\angle \bar{I}_{2STTF}$ now varies around the 0° axis, which is the axis of the faulty phase A. For the cases of faulty phase B, the angle was around 120° , thus validating the phase location procedure.

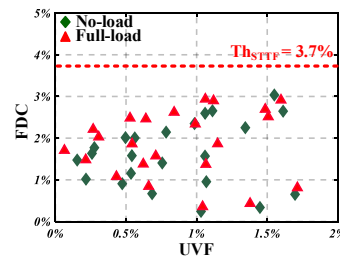


Fig. 8. FDC values with the healthy motor at no-load and full-load conditions for different permissible UVF values.

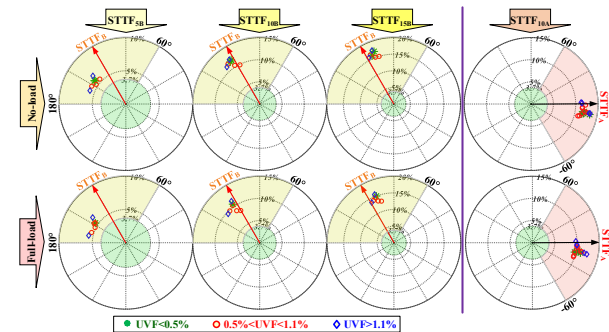


Fig. 9. FDC and $\angle \bar{I}_{2STTF}$ for no-load (top) and full-load (down) conditions, corresponding to $STTF_{5B}$, $STTF_{10B}$ and $STTF_{15B}$ (1st ~ 3rd col.), and $STTF_{10A}$ (4th col.), with different UVFs up to 1.7% .

4.6. STTF Detection for Inverter-Fed Machines

To evaluate the proposed diagnostic methodology in inverter-fed machines, the same WRIM was supplied by an inverter and the obtained drive system was operated in scalar control mode. In these conditions, the motor supply voltages are roughly symmetrical, consequently, there is no need to calculate the component \bar{I}_{2n} due to unbalanced voltage sources. However, the measured current \bar{I}_2 is not null even when the machine is in healthy conditions, due to its intrinsic constructional asymmetries. The obtained results for different STTFs in phases A and B, at different supply frequencies ranging from 20 up to 60 Hz, are shown in Fig. 10 and Table III. The results show that with

the machine in healthy conditions, the FDC value is lower than 1.2%, then increasing with the number of shorted turns. The STTFs are detectable with higher resolution at higher frequencies, as expected, due to the higher short-circuit current for higher frequencies (which leads to higher induced voltages).

In comparison with the line-fed case, for the same number of shorted turns, the method seems to have a higher sensitivity for the inverter-fed machine. In terms of fault location, as shown in Table III, the angle $\angle \bar{I}_{2STTF}$ allows a correct identification of the faulty phase, as demonstrated before for the line-fed situation.

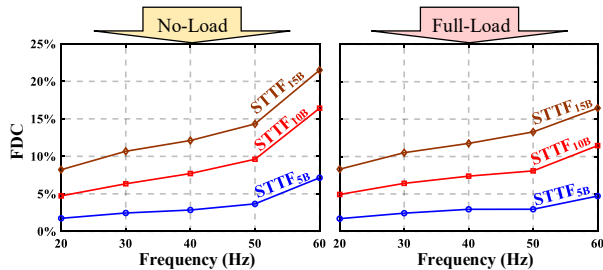


Fig. 10. FDC versus the applied frequency for several numbers of shorted turns at no-load (left) and full-load (right) conditions.

Table III. Identification of the faulty phase through $\angle \bar{I}_{2STTF}$

Load Condition	f (Hz)	$\angle \bar{I}_{2STTF}$ (Deg.)			
		STTF _{5A}	STTF _{10A}	STTF _{5B}	STTF _{10B}
No-load	20	9.7	3.0	106.7	112.9
	30	7.7	-1.6	114.0	114.3
	40	6.6	-2.5	117.6	115.9
	50	7.3	1.7	128.8	122.0
	60	6.3	-8.7	130.7	114.0
Full-load	20	8.5	2.2	110.5	113.3
	30	6.0	-2.4	117.6	115.2
	40	5.0	-3.5	121.7	116.7
	50	3.2	-2.8	139.7	116.8
	60	8.4	-13.5	133.8	114.7

5. Conclusion

A comprehensive stator turn-to-turn fault diagnostic algorithm based on the negative sequence equivalent model is presented in this paper, which has the capability of fault detection and faulty phase identification in online conditions. With this reliable method, the effect of the negative sequence voltage component is eliminated. Moreover, the threshold level to detect STTF is obtained based on the actual construction of the machine (considering its inherent asymmetries), using a simple and straightforward procedure.

The experimental results have shown that from the sensitivity point of view, even weak faults with five shorted turns (2.3% of the total number of turns per phase) are detectable in the tested machine.

The robustness and security of this technique against unbalanced voltage sources with a permissible unbalance factor up to 1.7%, and load level variations from no-load up to full-load conditions were also demonstrated, making it a sensitive, reliable and secure non-invasive diagnostic method. Also, the performance of this method for the inverter-fed mode showed that the related sensitivity will be increased in such a condition.

6. References

- [1] T. Javied, T. Rackow, R. Stankalla, C. Sterk, and J. Franke, "A study on electric energy consumption of manufacturing companies in the German industry with the focus on electric drives," *Procedia CIRP*, vol. 41, pp. 318-322, Jan. 2016.
- [2] M. Kostic, M. Ivanovic, and S. Minic, "Reduction of electric energy consumption in induction motor drives by setting supply voltage," in *2012 2nd International Symposium On Environment Friendly Energies And Applications*, June. 2012, Newcastle upon Tyne, UK, pp. 128-133: IEEE, doi: 10.1109/EFEA.2012.6294073.
- [3] B. Venkataraman, B. Godsey, W. Premerlani, E. Shulman, M. Thaku, and R. Midence, "Fundamentals of a motor thermal model and its applications in motor protection," in *58th Annual Conference for Protective Relay Engineers*, Apr. 2005, College Station, TX, USA, pp. 127-144: IEEE, doi: 10.1109/CPRE.2005.1430428.
- [4] S. Cho, J. H. Shin, H. B. Jun, H. J. Hwang, C. Ha, and J. H. Wang, "A study on estimating the next failure time of compressor equipment in an offshore plant," *Mathematical Problems in Engineering*, vol. 2016, p. 14, Oct. 2016.
- [5] J. Vico and R. Hunt, "Principles in motor protection," *IEEE Industry Applications Magazine*, vol. 17, no. 6, pp. 52-61, Dec. 2011.
- [6] M. R. W. Group, "Report of large motor reliability survey of industrial and commercial installations, Part I," *IEEE Trans. Industrial Applications*, vol. IA-21, no. 4, pp. 853-864, Aug. 1985.
- [7] R. M. Tallam, T. G. Habetler, and R. G. Harley, "Transient model for induction machines with stator winding turn faults," *IEEE Transactions on Industry Applications*, vol. 38, no. 3, pp. 632-637, June 2002.
- [8] IEEE Recommended Practice for Conducting Short-Circuit Studies and Analysis of Industrial and Commercial Power Systems, *IEEE Std 3002.3-2018*, pp. 1-184, Mar. 2019.
- [9] G. Mirzaeva and K. I. Saad, "Advanced diagnosis of stator turn-to-turn faults and static eccentricity in induction motors based on internal flux measurement," *IEEE Transactions on Industry Applications*, vol. 54, no. 4, pp. 3961-3970, Aug. 2018.
- [10] F. Trutt, J. Sottile, and J. L. Kohler, "Condition monitoring of induction motor stator windings using electrically excited vibrations," in *Conference Record of the 2002 IEEE Industry Applications Conference. 37th IAS Annual Meeting (Cat. No. 02CH37344)*, Oct. 2002, Pittsburgh, PA, USA, vol. 4, pp. 2301-2305: IEEE, doi: 10.1109/IAS.2002.1042767.
- [11] G. Gentile, S. Meo, and A. Ometto, "Induction motor current signature analysis to diagnostics, of stator short circuits," in *4th IEEE International Symposium on Diagnostics for Electric Machines, Power Electronics and Drives (SDMPED)*, Aug. 2003, Atlanta, GA, USA, pp. 47-51: IEEE, doi: 10.1109/DEMPED.2003.1234545.
- [12] J. H. Jung, J. J. Lee, and B. H. Kwon, "Online diagnosis of induction motors using MCSA," *IEEE Transactions on Industrial Electronics*, vol. 53, no. 6, pp. 1842-1852, Dec. 2006.
- [13] S. M. Cruz and A. M. Cardoso, "Diagnosis of stator inter-turn short circuits in DTC induction motor drives," *IEEE Transactions on Industry Applications*, vol. 40, no. 5, pp. 1349-1360, Oct. 2004.
- [14] A. M. Cardoso, S. Cruz, and D. Fonseca, "Inter-turn stator winding fault diagnosis in three-phase induction motors, by Park's vector approach," *IEEE Transactions on Energy Conversion*, vol. 14, no. 3, pp. 595-598, Sep. 1999.
- [15] S. M. Cruz and A. M. Cardoso, "Stator winding fault diagnosis in three-phase synchronous and asynchronous motors, by the extended Park's vector approach," *IEEE Transactions on industry applications*, vol. 37, no. 5, pp. 1227-1233, Oct. 2001.
- [16] S. M. Cruz, "An active-reactive power method for the diagnosis of rotor faults in three-phase induction motors operating under time-varying load conditions," *IEEE Transactions on Energy Conversion*, vol. 27, no. 1, pp. 71-84, Mar. 2012.
- [17] R. Maier, "Protection of squirrel-cage induction motor utilizing instantaneous power and phase information," *IEEE Transactions on Industry Applications*, vol. 28, no. 2, pp. 376-380, Apr. 1992.
- [18] B. Wang, C. Shen, K. Xu, and T. Zheng, "Turn-to-turn short circuit of motor stator fault diagnosis in continuous state based on deep auto-encoder," *IET Electric Power Applications*, vol. 13, no. 10, pp. 1598-1606, Oct. 2019.

- [19] R. M. Tallam, T. G. Habetler, and R. G. Harley, "Self-commissioning training algorithms for neural networks with applications to electric machine fault diagnostics," *IEEE Transactions on Power Electronics*, vol. 17, no. 6, pp. 1089-1095, Nov. 2002.
- [20] I. P. T. Soumas, G. Georgoulas, E. D. Mitronikas, and A. N. Safacas, "Asynchronous machine rotor fault diagnosis technique using complex wavelets," *IEEE Transactions on Energy Conversion*, vol. 23, no. 2, pp. 444-459, June. 2008.
- [21] G. A. Jimenez, A. O. Munoz, and M. A. Duarte-Mermoud, "Fault detection in induction motors using Hilbert and Wavelet transforms," *Electrical Engineering*, vol. 89, no. 3, pp. 205-220, Jan. 2007.
- [22] B. A. Vinayak, K. A. Anand, and G. Jagadanand, "Wavelet-based real-time stator fault detection of inverter-fed induction motor," *IET Electric Power Applications*, vol. 14, no. 1, pp. 82-90, Jan. 2020.
- [23] A. Siddique, G. Yadava, and B. Singh, "Effects of voltage unbalance on induction motors," in *Conference Record of the 2004 IEEE International Symposium on Electrical Insulation*, Sep. 2004, Indianapolis, IN, USA, pp. 26-29: IEEE, doi: 10.1109/ELINSL.2004.1380430.
- [24] *IEEE Guide for AC Motor Protection IEEE Std C37.96-2012 (Revision of IEEE Std C37.96-2000)*, pp. 1-160, Feb. 2013.
- [25] A. Von Jouanne and B. Banerjee, "Assessment of voltage unbalance," *IEEE transactions on power delivery*, vol. 16, no. 4, pp. 782-790, Oct. 2001.
- [26] S. Williamson and K. Mirzozian, "Analysis of cage induction motors with stator winding faults," *IEEE transactions on power apparatus and systems*, vol. PAS-104, no. 7, pp. 1838-1842, July 1985.
- [27] G. Kliman, W. Premerlani, R. Koegl, and D. Hoeweler, "A new approach to on-line turn fault detection in AC motors," in *IAS'96. Conference Record of the 1996 IEEE Industry Applications Conference 31st IAS Annual Meeting*, Oct. 1996, San Diego, CA, USA, vol. 1, pp. 687-693: IEEE, doi: 10.1109/IAS.1996.557113.
- [28] F. Ghassemi and M. Perry, "Review of voltage unbalance limit in the GB grid code CC. 6.1. 5 (b)," *National Grid, Report*, pp. 14-58, Oct. 2014.
- [29] H. A. Toliyat and G. B. Kliman, *Handbook of electric motors*. CRC press, Oct. 2018.
- [30] J. Sottile, F. C. Trutt, and J. L. Kohler, "Condition monitoring of stator windings in induction motors. II. Experimental investigation of voltage mismatch detectors," *IEEE Transactions on Industry Applications*, vol. 38, no. 5, pp. 1454-1459, Oct. 2002.
- [31] F. C. Trutt, J. Sottile, and J. L. Kohler, "Online condition monitoring of induction motors," *IEEE Transactions on Industry Applications*, vol. 38, no. 6, pp. 1627-1632, Dec. 2002.
- [32] S. B. Lee, R. M. Tallam, and T. G. Habetler, "A robust, online turn-fault detection technique for induction machines based on monitoring the sequence component impedance matrix," *IEEE Transactions on Power Electronics*, vol. 18, no. 3, pp. 865-872, May. 2003.
- [33] S. Cheng, P. Zhang, and T. G. Habetler, "An impedance identification approach to sensitive detection and location of stator turn-to-turn faults in a closed-loop multiple-motor drive," *IEEE Transactions on Industrial Electronics*, vol. 58, no. 5, pp. 1545-1554, May 2011.
- [34] A. Berzoy, A. A. Mohamed, and O. Mohammed, "Complex-vector model of interturn failure in induction machines for fault detection and identification," *IEEE Transactions on Industry Applications*, vol. 53, no. 3, pp. 2667-2678, May 2017.
- [35] A. Berzoy, H. H. Eldeeb, and O. A. Mohammed, "Online detection of stator faults in DTC-driven IM using SC impedance matrix off-diagonal term," *IEEE Transactions on Industry Applications*, vol. 55, no. 6, pp. 5906-5915, Dec. 2019.
- [36] M. Arkan, D. Perović, and P. Unsworth, "Online stator fault diagnosis in induction motors," *IEE Proceedings-Electric Power Applications*, vol. 148, no. 6, pp. 537-547, Nov. 2001.
- [37] M. Arkan, D. Kostic-Perovic, and P. Unsworth, "Modelling and simulation of induction motors with inter-turn faults for diagnostics," *Electric Power Systems Research*, vol. 75, no. 1, pp. 57-66, July 2005.
- [38] M. Arkan and P. Unsworth, "Stator fault diagnosis in induction motors using power decomposition," in *Conference Record of the 1999 IEEE Industry Applications Conference. 34th IAS Annual Meeting (Cat. No. 99CH36370)*, Oct. 1999, Phoenix, AZ, USA, vol. 3, pp. 1908-1912: IEEE, doi: 10.1109/IAS.1999.805999.
- [39] M. Bouzid and G. Champenois, "Accurate stator fault detection insensitive to the unbalanced voltage in induction motor," in *2012 XXth International Conference on Electrical Machines*, Sep. 2012, Marseille, France, pp. 1545-1551: IEEE, doi: 10.1109/ICEIMach.2012.6350084.
- [40] M. Bouzid and G. Champenois, "A novel reliable indicator of stator windings fault in induction motor extracted from the symmetrical components," in *2011 IEEE International Symposium on Industrial Electronics*, June 2011, Gdansk, Poland, pp. 489-495: IEEE, doi: 10.1109/ISIE.2011.5984074.
- [41] M. B. K. Bouzid and G. Champenois, "New expressions of symmetrical components of the induction motor under stator faults," *IEEE Transactions on Industrial Electronics*, vol. 60, no. 9, pp. 4093-4102, Sep. 2013.
- [42] S. Bakhri, N. Ertugrul, and W. L. Soong, "Negative sequence current compensation for stator shorted turn detection in induction motors," in *IECON 2012 - 38th Annual Conference on IEEE Industrial Electronics Society*, Oct. 2012, Montreal, QC, Canada, pp. 1921-1926: IEEE, doi: 10.1109/IECON.2012.6388908.
- [43] R. M. Tallam, T. G. Habetler, R. G. Harley, D. J. Gritter, and B. H. Burton, "Neural network based online stator winding turn fault detection for induction motors," in *Conference Record of the 2000 IEEE Industry Applications Conference. 35th IAS Annual Meeting and World Conference on Industrial Applications of Electrical Energy (Cat. No. 00CH37129)*, Oct. 2000, Rome, Italy, vol. 1, pp. 375-380: IEEE, doi: 10.1109/IAS.2000.881138.
- [44] R. M. Tallam, T. G. Habetler, and R. G. Harley, "Continual online training of neural networks with applications to electric machine fault diagnostics," in *2001 IEEE 32nd Annual Power Electronics Specialists Conference (IEEE Cat. No. 01CH37230)*, June 2001, Vancouver, BC, Canada, vol. 4, pp. 2224-2228: IEEE, doi: 10.1109/PESC.2001.954450.
- [45] R. M. Tallam, T. G. Habetler, and R. G. Harley, "Experimental testing of a neural-network-based turn-fault detection scheme for induction machines under accelerated insulation failure conditions," in *4th IEEE International Symposium on Diagnostics for Electric Machines, Power Electronics and Drives (SDMPED)*, Aug. 2003, Atlanta, GA, USA, pp. 58-62: IEEE, doi: 10.1109/DEMPED.2003.1234547.
- [46] M. A. Cash, T. G. Habetler, and G. B. Kliman, "Insulation failure prediction in AC machines using line-neutral voltages," *IEEE Transactions on Industry Applications*, vol. 34, no. 6, pp. 1234-1239, Dec. 1998.
- [47] J. L. Kohler, J. Sottile, and F. C. Trutt, "Alternatives for assessing the electrical integrity of induction motors," *IEEE Transactions on Industry Applications*, vol. 28, no. 5, pp. 1109-1117, Oct. 1992.
- [48] J. L. Kohler, J. Sottile, and F. C. Trutt, "Condition monitoring of stator windings in induction motors. I. Experimental investigation of the effective negative-sequence impedance detector," *IEEE Transactions on Industry Applications*, vol. 38, no. 5, pp. 1447-1453, Oct. 2002.
- [49] *IEEE Standard Test procedure for Polyphase Induction Motors and Generators, IEEE Std 112-2017 (Revision of IEEE Std 112-2004)*, pp. 1-115, Feb. 2018.
- [50] D. Yazdani, M. Mojiri, A. Bakhshai, and G. Joos, "A fast and accurate synchronization technique for extraction of symmetrical components," *IEEE Transactions on Power Electronics*, vol. 24, no. 3, pp. 674-684, Mar. 2009.
- [51] *IEEE Standard Electrical Power System Device Function Numbers, Acronyms, and Contact Designations, IEEE Std C37.2-2008 (Revision of IEEE Std C37.2-1996)*, pp. 1-48, Oct. 2008.